Catalysis Today 141 (2009) 103–108

Contents lists available at ScienceDirect

Catalysis Today

journal homepage: www.elsevier.com/locate/cattod

# Probing the Fe(III) sites in mesoporous FeMCM-41

Sushanta K. Badamali [a], Parasuraman Selvam [b,*]

[a] Department of Chemistry, North Orissa University, Baripada, 757 003 Orissa, India
[b] National Center for Catalysis Research, Department of Chemistry, Indian Institute of Technology-Madras, Chennai 600 036, India

Dedicated to Dr. Paul Ratnasamy on the occasion of his 65th birthday.

ARTICLE INFO

*Article history:*
Available online 24 June 2008

*Keywords:*
FeMCM-41
$^{29}$Si MAS-NMR
Trivalent iron
Microwave variation EPR

ABSTRACT

Spectroscopic techniques such as $^{29}$Si MAS-NMR, Mössbauer, magnetic susceptibility, EPR and microwave variation EPR studies were used in order to study the location, coordination, oxidation state and stability of trivalent in FeMCM-41. $^{29}$Si MAS-NMR studies revealed that paramagnetic Fe(III) is present in the direct vicinity of [$SiO_4$] tetrahedral and therefore results in broadening of spectral lines. Absence of side spinning bands are attributed to the uniform dispersion of $Fe_xO_y$ within the matrix. Observed isomer shift value of $<$0.3 mm/s and the appearance of sexset pattern in Mössbauer spectrum is attributed to the tetrahedral coordination of Fe(III) and superparamagnetic $Fe_xO_y$ nanoparticles, respectively. The co-existence of paramagnetic and superparamagnetic Fe(III) is also inferred from magnetic susceptibility studies. Analysis of EPR spectrum indicated that Fe(III) is present in two different tetrahedral sites along with octahedral coordination [S.K. Badamali, A. Sakthivel, P. Selvam, Catal. Lett. 65 (2000) 153]. Room temperature microwave power variation electron paramagnetic resonance (EPR) (0.5–10 mW) studies are in good agreement with above interpretations. During template removal, Fe(III) is preferably dislodged from the distorted framework sites irrespective of calcination temperature. The population of unsymmetrical Fe(III) species is inferred to be relatively less as compared to the symmetrical sites, in the calcined form.

© 2008 Elsevier B.V. All rights reserved.

## 1. Introduction

It is of considerable interest to develop molecular sieve-based solid acid catalysts that may replace the conventionally used hazardous non-selective homogeneous catalysts for alkylation, acylation, benzoylation and sulfonation, etc. [1]. In this regard, trivalent iron-containing zeolite and zeolite-like molecular sieves are of special interest due to their application as solid acid catalyst as well as red–ox catalyst [2]. With the advent of mesoporous materials (M41S family) in 1992 [3] and possible incorporation of trivalent iron into the framework has further broadened the scope of applications [4–6]. Often the location, coordination, stability and oxidation state of trivalent iron in the zeolitic matrix is often a subject of considerable discussion as these parameters directly influence the catalytic performance. The study of the active sites in ferrislicates is challenging due to the complex Fe(III) chemistry under synthesis conditions [2]. Nevertheless, Fe(III) being a paramagnetic ion ($d^5$ system) a variety of techniques can be employed to probe the Fe(III) sites in ferrisilicate molecular sieves. In continuation to our earlier work on FeMCM-41 [7–10] and FeMCM-48 [11] materials, herein, we report on the location, coordination and stability of Fe(III) sites, which are inferred from a various spectroscopic techniques, viz., $^{29}$Si magic angle spinning-nuclear magnetic resonance (MAS-NMR), Mössbauer, magnetic susceptibility, electron paramagnetic resonance (EPR) and microwave power variation EPR studies.

## 2. Experimental

The FeMCM-41 samples were synthesized hydrothermally, as per the procedure reported elsewhere [8], with a gel composition of 1 $SiO_2$:0.5 NaOH:0.5 CTAB:(0–0.1) $Fe_2O_3$:(0.108–0.149) $H_2SO_4$:68 $H_2O$. The number within the parentheses represents the silicon-to-iron content in molar gel composition. The gel (pH $\sim$ 11.5) was kept in a Teflon-lined autoclaves and heated in air oven at 423 K for 9 days. The crystallized products were washed and filtered and are designated as sodium-form of as-synthesized (Na–FeMCM-41) samples. This sample was then calcined in a tubular furnace at 773 K under nitrogen atmosphere for 3 h followed by 6 h in air. The sodium form of the ironsilicate was converted into acidic form, viz., H-FeMCM-41, by repeated ion-exchange procedure.

* Corresponding author. Tel.: +91 44 2257 4235; fax: +91 44 2257 4202.
*E-mail address:* selvam@iitm.ac.in (P. Selvam).

0920-5861/$ – see front matter © 2008 Elsevier B.V. All rights reserved.
doi:10.1016/j.cattod.2008.05.007

All the samples were systematically characterized by various analytical, e.g., powder X-ray diffraction (XRD), thermogravimetry–differential thermal analysis (TG–DTA), Brunauer–Emmett–Teller (BET) surface area and temperature-programmed desorption (TPD) of ammonia, and spectroscopic, viz., Fourier transform-infrared (FT-IR), Diffuse reflectance ultraviolet-visible (DRUV-vis), EPR, inductively coupled plasma-atomic emission (ICP-AES), techniques. Further experimental details can be seen elsewhere [8].

The samples were further studied in detail by MAS-NMR and Mössbauer spectroscopy as well as magnetic susceptibility measurements. $^{29}$Si MAS-NMR spectra of various samples were recorded on a Varian VXR-300S spectrometer with a Doty Scientific CP-MAS probe. The frequency used was 121.42 MHz. Forty-five pulses were used for all measurements with repetition time of 10 s. Data were obtained at a MAS speed of 4.5 kHz and tetramethylsilane was employed as the reference. Mössbauer spectral measurement was performed in transmission geometry with 2.0 GBq, equipped with a $^{57}$Co source in a rhodium matrix on a Ranger MS900 spectrometer. Probability distribution of the hyperfine magnetic field was calculated from an experimental Mössbauer spectrum with software developed by Le Caer. A Lorenzian function was assumed for the line shape. The calculation was performed in a hyperfine magnetic field of 0–60 T intervals. The low temperature (4–300 K) spectra were recorded with a Ranger electronics MS-700 MR spectrometer with speed of −10 to +10 mm s$^{-1}$.

Magnetic susceptibility ($\chi$) was measured using commercial superconducting quantum interference device magnetometer (DC squid; quantum design model MPMS) in the temperature range of 5–300 K. The temperature dependence of the $\chi$ obtained was expressed as $\chi_0 + [C/(T-\theta)]$, where $\chi_0$ is the temperature independent component of the susceptibility and $C/(T-\theta)$ is the Curie–Weiss contribution. EPR spectra of FeMCM-41 were recorded on a Varian (E-line Century series E-112) spectrometer with 100 kHz field modulation. The magnetic field was calibrated with a proton resonance meter and tetracyanoethylene ($g = 2.0077$) as a reference. The microwave power variation EPR signals were obtained by varying power between 0.5 and 10 mW. The experimental parameters such as temperature, amount of sample, sample container, the EPR cavity, modulation frequency, and scan range were kept identical to ensure the accuracy of the experimental data.

## 3. Results and discussion

The powder XRD, BET surface area and TG–DTA analyses (not reproduced here) indicted the mesoporous nature of the FeMCM-41 samples which is in line with the earlier reports [7]. Further, the isomorphous substitution of Fe(III) in the framework positions was supported by FT-IR, DRUV-vis, and EPR studies (note reproduced here). Table 1 lists the lattice parameter of different FeMCM-41 samples synthesized with various Si/Fe (molar) ratios. The observed decrease in the $a_0$ values for the calcined samples compared to the as-synthesized counter parts could be attributed to the shrinkage of the lattice as a consequence of the removal of template molecules. It can also be seen from Table 1 that the Si/Fe (molar ratio) in the calcined samples is considerably reduced. This decrease is attributed to silicon deficit in the sample, which could possible due to the incomplete (poly) condensation of silicon precursor. This may, however, be present as soluble species in mother liquor of the synthesized samples and subsequently removed during washing of the crystallized products. The sample FeMCM-41(50) possesses a surface area of 637 m$^2$ g$^{-1}$, which falls in the range of typical mesoporous materials. However, the lower value as compared to its siliceous analogues could be accounted to the blocking of the mesopores partially by (non-framework) iron oxide nanoparticles produced upon calcinations as well as the lack of long range ordering along the pore channel walls [7].

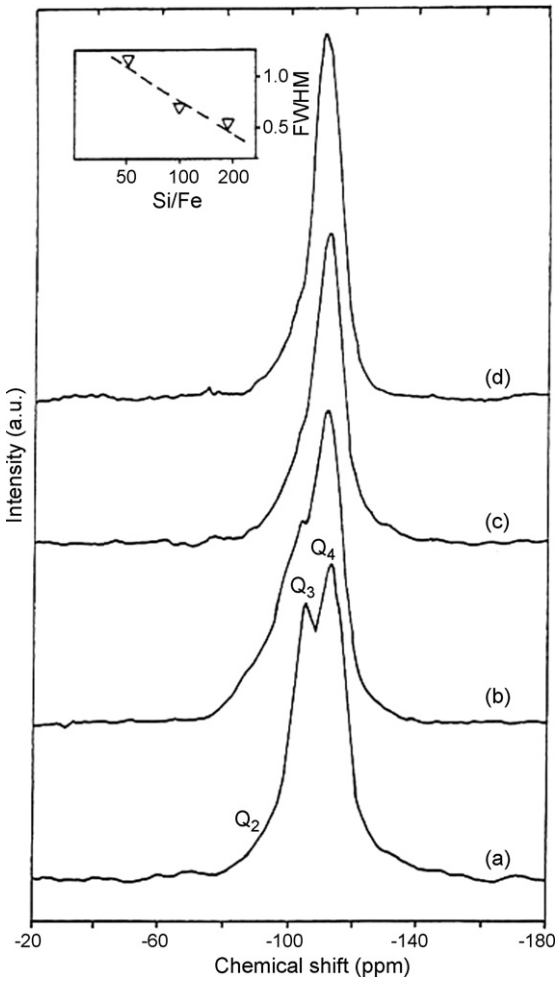


**Fig. 1.** $^{29}$Si MAS-NMR spectra of as-synthesized: (a) MCM-41; (b) FeMCM-41(50); (c) FeMCM-41(100); (d) FeMCM-41(200).

### 3.1. $^{29}$Si MAS-NMR studies

$^{29}$Si MAS-NMR spectra of as-synthesized and calcined FeMCM-41 samples with varying Si/Fe content are shown in Figs. 1 and 2,

**Table 1**
Synthesis, structural and textural data of FeMCM-41

| Sample | ICP-AES (Si/Fe molar ratio) | | XRD, $a_0$ (Å) | | BET surface area (m$^2$ g$^{-1}$) |
|---|---|---|---|---|---|
| | Sample gel | Calcined product | Synthesis sample | Calcined sample | |
| MCM-41 ($\propto$) | $\propto$ | $\propto$ | 45.91 | 41.78 | 900 |
| FeMCM-41 (200) | 200 | 172 | 52.00 | 50.65 | – |
| FeMCM-41 (100) | 100 | 72 | 53.65 | 52.54 | – |
| FeMCM-41 (50) | 50 | 30 | 57.91 | 57.26 | 637 |

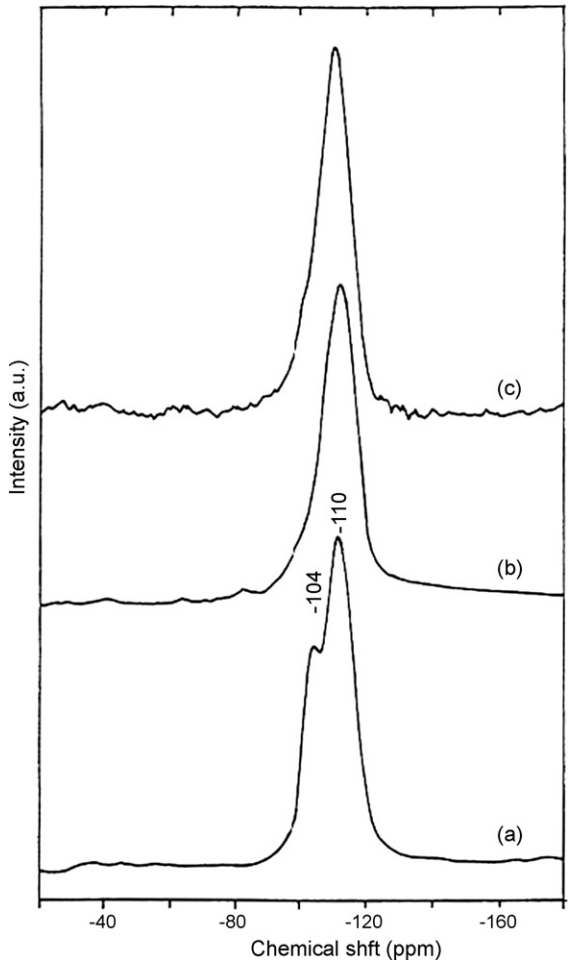


**Fig. 2.** $^{29}$Si MAS-NMR spectra of calcined: (a) MCM-41; (b) FeMCM-41(200); (c) FeMCM-41(100).

respectively. For a comparison the spectrum of siliceous MCM-41 is included. As-synthesized MCM-41 exhibits signals at −103 and −109 ppm assigned to $Q_3$(≡Si–OH) and $Q_4$(Si(–OSi)$_4$) sites, respectively [12]. However, the intensity of $Q_3$ signal in FeMCM-41 is considerably decreased along with line broadening. Such behaviour indicates a direct interaction between paramagnetic Fe(III) and $Q_3$ sites (nuclear–electron coupling), i.e., as a consequence the relaxation time is shortened. This observation is in accordance with the earlier reports and attributed to the isomorphous substitution [13–16]. The presence of a shoulder at −103 ppm, clearly observed in all samples is tentatively assigned to Si(–O–Fe) linkage. Further, it can also be seen from figure that the full width at half maxima (FWHM) of $^{29}$Si signal increases linearly with increasing iron content in FeMCM-41 (see inset, Fig. 2) implying a uniform dispersion and high degree of spatial ordering of Fe(III) species [13]. Sample having the highest iron content (i.e., Si/Fe = 50) showed significant line broadening along with good signal intensity for $Q_3$ sites. Presumably, the insertion of Fe(III) in the silicon framework distorts the $[SiO_4]^{4-}$ geometry, and hinders the condensation of silanol groups as observed in FeMCM-48 [16]. A close inspection of the spectra of calcined samples revealed that the broadening is lower than the as-synthesized analogues suggesting that part of the Fe(III) ions have remained in the framework [15]. The absence of spinning side bands in all these samples is due to weak dipole–dipole interactions/due to high dispersion of Fe(III) species [17,18].

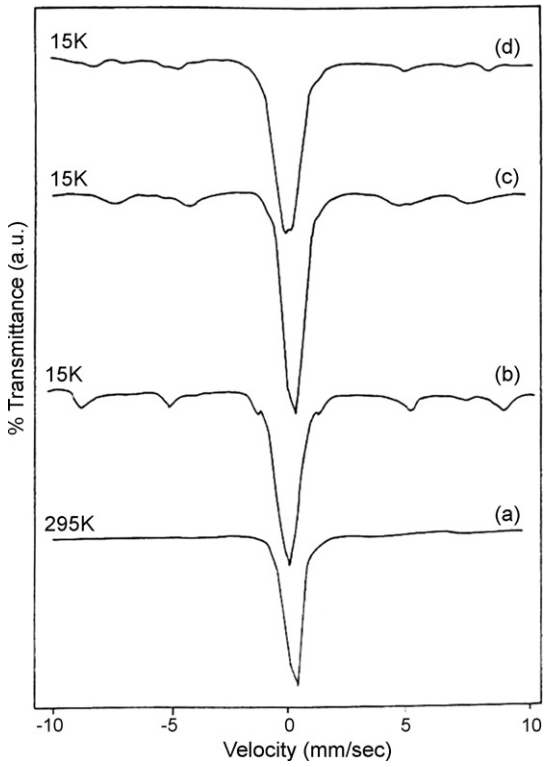


**Fig. 3.** Mössbauer spectra of as-synthesized: (a) FeMCM-41(50); (b) FeMCM-41(50); (c) FeMCM-41(100); (d) FeMCM-41(200).

### 3.2. Mössbauer studies

Mössbauer spectra of different as-synthesized FeMCM-41 samples are shown in Fig. 3. The room temperature spectrum of FeMCM-41(50) showed a singlet with isomeric shift value of 0.26 mm s$^{-1}$ and quadrupole splitting, <0.5 mm s$^{-1}$, relative to metallic iron. This indicates presence of paramagnetic Fe(III) in tetrahedral coordination. However, the spectrum recorded at 15 K showed a six-line pattern along with a strong quadrupole doublet. The presence of doublet pattern is attributed to the high spin Fe(III) in the tetrahedral framework. On the other hand, the sexset pattern is typical characteristics of superparamagnetic particles, observed at low temperature [19,20]. In fact Bachari et al. [19] have attributed the sexset pattern to superparamagnetic iron oxide nanoparticles having a diameter of 1–3 nm in a related mesoporous material. Close inspection of the spectrum suggests that there may be two sets of six magnetic hyperfine resonance lines. This arises due to the formation of FeO(OH) and $Fe_2O_3$ nanoparticles from the precipitated Fe(OH)$_3$ under reaction (alkaline) conditions [21,22]. The low temperature spectra of different FeMCM-41 samples are composed of both quadrupole doublets and sexset pattern corresponding to paramagnetic and superparamagnetic Fe(III) species, respectively. At this juncture it also noteworthy that one of the major problems associated with nanoporous silicate materials is the instability of trivalent iron in the tetrahedral framework during heat treatment, which is in contrast with the corresponding aluminophosphate analogues [23]. Accordingly, they show more non-framework species. For example, the as-synthesized FeMCM-41 exhibits an isomer shift <0.3 mm s$^{-1}$ with narrow quadruple splitting indicating trivalent iron in tetrahedral environment, while the calcined FeMCM-41 with a shift >0.3 mm s$^{-1}$ and a broad quadruple splitting characterizes the six-coordinated iron species [23]. That is, the increase in isomer shift for the calcined sample indicates the formation of octahedral

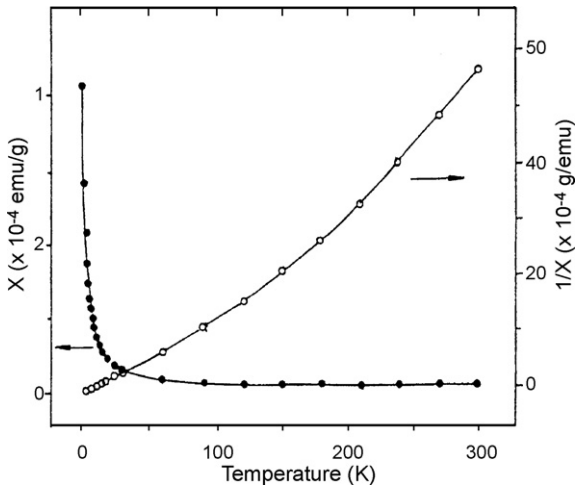


**Fig. 4.** Temperature dependence of magnetic susceptibility of as-synthesized FeMCM-41(50).

trivalent iron species as confirmed by the sexset pattern obtained at 4.2 K.

### 3.3. Magnetic susceptibility studies

The temperature dependence of the normal ($\chi$) and reciprocal ($1/\chi$) susceptibilities is shown in Fig. 4. The low temperature (<150 K) part of the Curie–Weiss fit, i.e., straight line passing through the origin is indicative of paramagnetic Fe(III) [20]. However, the upward bending of the curve at higher temperature (>150 K) is attributed to the dependence of spontaneous magnetization on temperature. That suggests the magnetic behaviour departs from paramagnetic nature due to the interaction between iron oxy and hydroxy clusters. These interpretations well support the co-existence of paramagnetic and superparamagnetic Fe(III) species in mesoporous FeMCM-41 [24].

### 3.4. EPR studies

Fig. 5 shows the EPR spectra of the as-synthesized FeMCM-41. As can be seen from this figure that the appearance of prominent signals at three distinct $g_{eff}$ values signifies the existence of trivalent iron in three different environments. At 77 K, the EPR signals show enhanced intensity and sharpness, which could be accounted for the reduced magnetic interaction between neighboring paramagnetic trivalent iron and/or less distortion in the local symmetry at low temperature. It is, however, interesting to note that upon calcination the intensity of lower field signal is significantly reduced (Fig. 6) while the signal intensity at higher field exhibits a small or no change. It is obvious that the distorted (framework) sites are less resistant to thermal treatment thereby partly dislodging from the framework upon calcinations which is in agreement with DRUV-vis studies. Similar EPR spectra were also obtained for the samples calcined at lower temperatures (Fig. 7). EPR spectra of FeMCM-41(50) sample calcined at different temperatures, $NH_4^+$-exchanged as well as in the $H^+$-form is included in Fig. 7. The typical first derivative EPR spectrum of FeMCM-41 shows three distinct signal centred at $g_{eff}$ = 4.3, 2.2 and 2.0, are attributed to Fe(III) in distorted tetrahedral, $Fe_xO_y$, and in symmetrical tetrahedral/octahedral coordination, respectively, as discussed in detail previously [8,25]. Interestingly, it has been observed that upon calcination partial dislodgement of Fe(III) occur from the framework [13] and it occupies the inner surface as $Fe_xO_y$ particles. Therefore, we have attempted to calcine the samples at different temperatures. However, it was difficult to

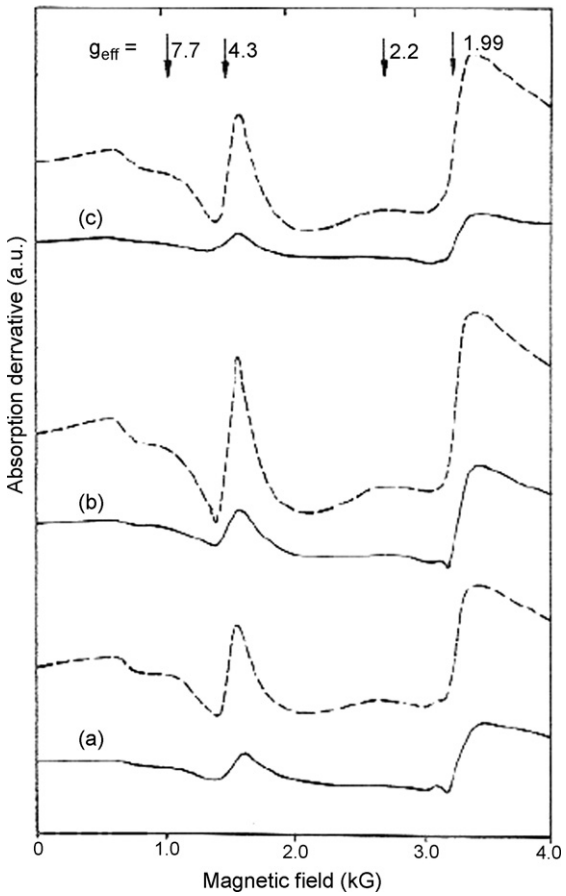


**Fig. 5.** EPR spectra of as-synthesized: (a) FeMCM-41(200); (b) FeMCM-41(100); (c) FeMCM-41(50). Solid line: data at 300 K; dashed line: data at 77 K.

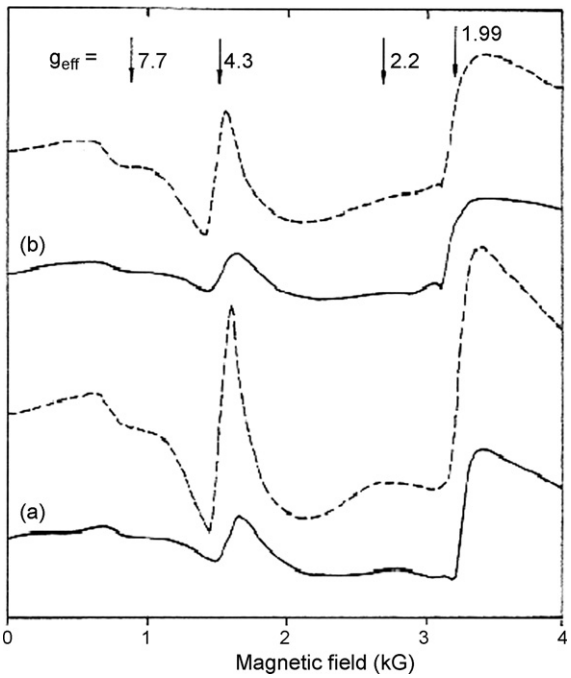


**Fig. 6.** EPR spectra FeMCM-41(100): (a) as-synthesized; (b) calcined. Solid line: data at 300 K; dashed line: data at 77 K.

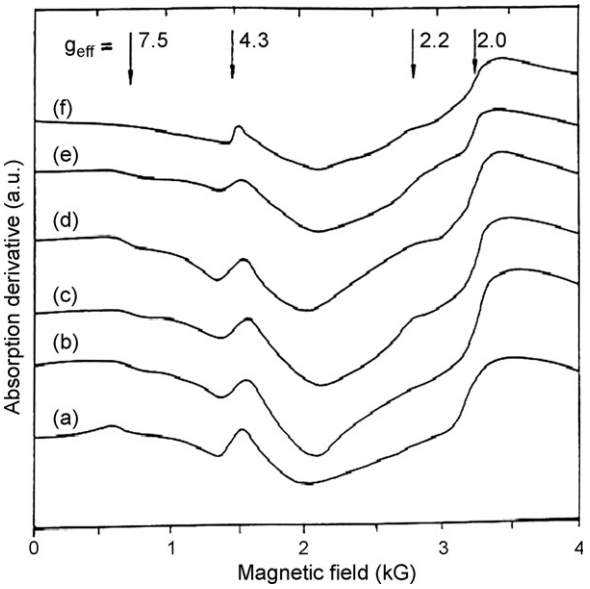


**Fig. 7.** EPR spectra of FeMCM-41(50) calcined at: (a) 823 K; (b) 773 K; (c) 723 K; (d) 673 K; (e) $NH_4^+$-FeMCM-41(50); (f) $H^+$-FeMCM-41(50).

prevent the dislodgement. This is quite understandable, as larger trivalent iron (crystal radii = 0.63 Å) is comparatively unstable in the tetrahedral framework of tetravalent silicon (crystal radii = 0.40 Å). Post-synthetic treatments, such as $NH^+$-ion exchange and thermal activation is often performed to obtain the $H^+$-FeMCM-41, which is employed as a potential acid catalyst [18]. Therefore, we extended our study to investigate the stability of different Fe(III) sites, during these treatments. It was noticed that upon $NH_4^+$ ion-exchange the signal intensities are decreased, indicating dislodgement of Fe(III) from framework sites, owing to the possible hydrolysis of Si–O–Fe or Si–O–Si linkages. Despite of partial dislodgement, in the protonated form ($H^+$-FeMCM-41)

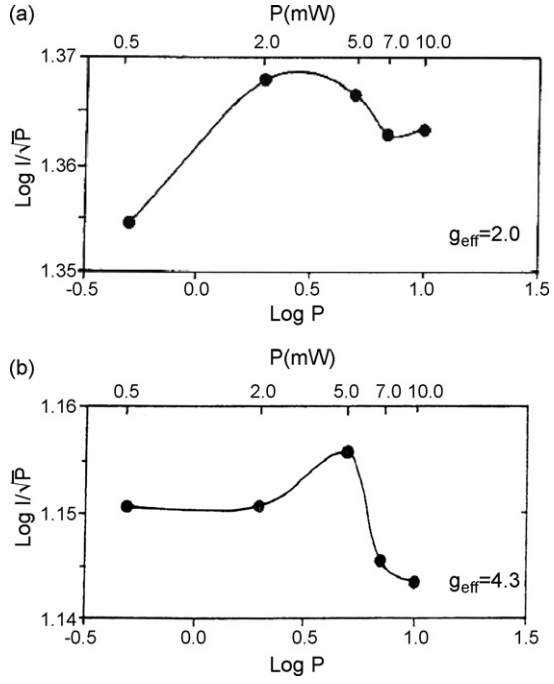


**Fig. 8.** Microwave saturation plots of as-synthesized FeMCM-41(50); (a) $g_{eff}$ = 2.0; (b) $g_{eff}$ = 4.3.

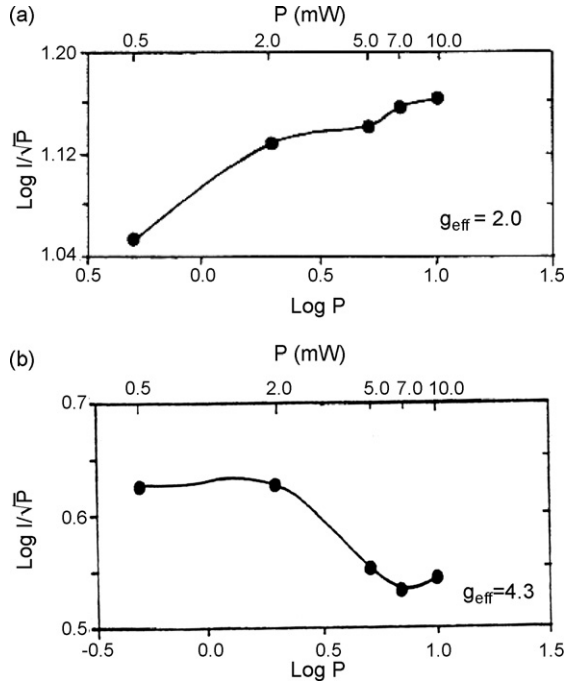


**Fig. 9.** Microwave saturation plots of calcined FeMCM-41(50): (a) $g_{eff}$ = 2.0 and (b) $g_{eff}$ = 4.3.

significant amount of Fe(III) still remains in the tetrahedral coordination and exhibits moderate-to-strong acidity [9].

EPR studies were further extended for MW power variation studies. The signals both at lower ($g_{eff}$ = 4.3) and higher field ($g_{eff}$ = 2.0) are chosen for microwave power studies as both are relevant to Fe(III) coordination and moreover narrow, hence convenient to study the signal intensity. For the as-synthesized sample, a plot of log ($I/\sqrt{P}$) vs. log $P$, for the signal at $g_{eff}$ = 2.0 showed saturation [26], i.e., shows a downward bending towards $x$-axis at $P \cong 4$ mW (Fig. 8a). On the contrary, the signal at $g_{eff}$ = 4.3 saturates between 5 and 7 mW (Fig. 8b). The saturation behaviour represents the equilibrium population of the paramagnetic species both in the ground and excited states. Saturation in the nearly same range of microwave power indicates that in the as-synthesized form, presumably both sites have nearly equal population.

It is, however, interesting to note that, the high field signal clearly showed non-saturation behaviour under the experimental microwave power variations (Fig. 9a). On the other hand, the low field signal showed a distinct saturation behaviour at $P < 2$ mW, in the calcined form (Fig. 9b). This could be attributed to the presence of higher number of paramagnetic Fe(III) sites, possibly in different coordination. The partial dislodgement of Fe(III) from the distorted framework and subsequent conversion to octahedral coordination adds up to the higher field signal intensity. The saturation of the $g_{eff}$ = 4.3 signal at lower microwave power as compared to the corresponding as-synthesized sample, further supports the decrease in the Fe(III) in the distorted framework position, upon calcination. These interpretations are in well agreement with other spectroscopic investigations reported previously [10].

## 4. Conclusion

The study of various measurements led us to the conclusion that paramagnetic Fe(III) substitutes isomorphously into the silicate framework of MCM-41 and remains both in distorted and symmetrical tetrahedral geometry. Tetrahedral Fe(III) sites are

in direct vicinity of silicon tetrahedral and thermally unstable, therefore, partly dislodged during calcination. Fe(III) located in extra-framework positions are more symmetric, stable and populated as compared to the framework analogues. Apart from this, Fe(III) is also present as superparamagnetic (oxy–hydroxy) nanoparticles and highly dispersed within mesopores. The different onset microwave power saturation indicated the population of these sites are also different. It is further envisaged that, as saturation behaviour is dependent of both relaxation processes and relaxation times, microwave power variation studies can be employed to derive other useful parameters pertaining to the paramagnetic metal centres in complex molecular sieve structures.

## Acknowledgement

The authors thank SAIF, IIT-Bombay for $^{29}$Si MAS-NMR and EPR measurements.

## References

[1] J.M. Thomas, Sci. Am. 266 (1992) 112.
[2] P. Ratnasamy, R. Kumar, Catal. Today 9 (1991) 329.
[3] J.S. Beck, J.C. Vartuli, W.T. Roth, M.E. Lenowicz, C.T. Kresge, K.D. Schmitt, C.T.W Chu, D.H. Olson, W.E. Sheppard, S.B. McCullen, J.B. Higgins, J.L. Schelnker, J. Am. Chem. Soc. 114 (1992) 10834.
[4] D. Trong On, D. Desplantier-Giscard, C. Danumah, S. Kaliaguine, Appl. Catal. A: Gen. 253 (2003) 545.
[5] N. Srinivas, V. Radharani, M. Radhakrishna, S.J. Kulkarni, K.V. Raghavan, J. Mol. Catal. A: Chem. 172 (2001) 187.
[6] M. Stockenhuber, R.W. Joyner, J.M. Dixon, M.J. Hudson, G. Grubert, Micropor. Mesopor. Mater. 44–45 (2001) 367.
[7] S.K. Badamali, P. Selvam, Stud. Surf. Sci. Catal. 113 (1998) 749.
[8] S.K. Badamali, A. Sakthivel, P. Selvam, Catal. Lett. 65 (2000) 153.
[9] S.K. Badamali, A. Sakthivel, P. Selvam, in: D. Do (Ed.), Adsorption Science Technology, World Scientific, Singapore, 2000, p. 553.
[10] P. Selvam, S.E. Dapurkar, S.K. Badamali, M. Murugasen, H. Kuwano, Catal. Today 68 (2001) 89.
[11] S.E. Dapurkar, S.K. Badamali, A. Sakthivel, P. Selvam, Bull. Catal. Soc. Ind. 4 (2005) 63.
[12] Q. Huo, D.I. Margolese, U. Ciesca, P. Feng, T.E. Gler, P. Sieger, R. Leon, P.M. Petroff, F. Schuth, G.D. Stucky, Nature 368 (1994) 317.
[13] V. Umamaheswari, W. Bohlmann, A. Poppl, A. Vinu, M. Hartmann, Micropor. Mesopor. Mater. 89 (2006) 47.
[14] W.J. Ball, J. Dwyer, A.A. Garforth, W.J. Smith, Stud. Surf. Sci. Catal. 28 (1986) 137.
[15] F. Testa, F. Crea, G.D. Diodati, L. Pasqua, R. Aiello, G. Terwagne, P. Lentz, J.B. Nagy, Micropor. Mesopor. Mater. 30 (1999) 187.
[16] H. Kosslick, G. Lische, H. Landmesser, B. Parlitz, W. Storek, R. Fricke, J. Catal. 176 (1998) 102.
[17] E. Oldfield, A.R. Kinsey, K.A. Smith, J.A. Nichols, R.J. Kirkpatrick, J. Magn. Res. 51 (1983) 325.
[18] H. Kosslick, G. Lische, G. Walther, A. Martin, R. Fricke, Micropor. Mater. 9 (1997) 13.
[19] K. Bachari, J.M.M. Millet, P. Bonville, O. Cherifi, F. Figueras, J. Catal. 249 (2007) 52.
[20] W. Kundig, H. Bommel, G. Constabaris, R.H. Lindguist, Phys. Rev. 142 (1996) 327.
[21] A. Vertes, K. Lazar, K. Kelemen, L. Bogucir, Radiochem. Radioanal. Lett. 4 (1970) 375.
[22] A. Lopez, F.J. Lazaro, J.L. Garcia-Palacios, A. Larrea, Q.A. Pankhurst, C. Martinez, A. Corma, J. Mater. Res. 12 (1997) 1519.
[23] P. Selvam, S.K. Mohapatra, J. Catal. 238 (2006) 88.
[24] P. Selvam, S.K. Badamali, M. Murugasen, H. Kuwano, in: V. Murugasan, B. Arabindoo, M. Palanichamy (Eds.), Recent Trends in Catalysis, Narosa, New Delhi, 1999, p. 533.
[25] D. Goldfarb, M. Bernardo, K.G. Strohmaier, D.E.W. Vayghan, H. Thomann, J. Am. Chem. Soc. 116 (1994) 6344.
[26] F.E. Mabbs, D. Collison, Electron Paramagnetic Resonance of d Transition Metal Compounds, Elsevier, Amsterdam, 1992.